Subcortical matter in the α-synucleinopathies spectrum: an MRI pilot study.

Gazzina S.[1], Premi E.[1], Turrone R.[1], Acosta-Cabronero J.[2], Rizzetti M.C.[3], Cotelli M.S.[4], Gasparotti R.[5], Padovani A.[6], Borroni B.[1]

[1] Centre for Ageing Brain and Neurodegenerative Disorders, University of Brescia, Brescia, Italy

[2] German Center for Neurodegenerative Diseases, Magdeburg, Germany

[3] S. Isidoro Hospital - FERB Onlus, Trescore Balneario, Bergamo, Italy

[4] Neurology Unit, Valle Camonica Hospital, Brescia, Italy

[5] Neuroradiology Unit, University of Brescia, Brescia, Italy

[6] Neurology Unit, Department of Clinical and Experimental Sciences, University of Brescia, Brescia, Italy

Word count: 3914

Abstract count: 190

Key words: Parkinson Disease, Lewy Body Dementia, basal ganglia, FIRST

Corresponding Author:

Barbara Borroni, MD

Neurology Unit, Department of Clinical and Experimental Sciences
University of Brescia
Piazza Spedali Civili 1, Brescia 25123, Italy
Email: bborroni@inwind.it

ABSTRACT

Introduction. α-synucleinopathies, such as Parkinson's Disease (PD) and Dementia with Lewy Bodies (DLB), are characterized by α-synuclein accumulation from brainstem structures to the neocortex. PD and DLB are clinically distinguishable, while discrimination between Parkinson Disease Dementia (PDD) and DLB can be subtle and based on the temporal relationship between motor and cognitive symptoms.

Objectives. To explore patterns of subcortical atrophy in PD, PDD and DLB, and assess specific differences between PD and PDD, and between DLB and PDD.

Methods. 16 PD, 11 PDD and 16 DLB patients were recruited and underwent 1.5 Tesla structural MRI scanning. Segmentation of subcortical structures was performed with a well-validated, fully-automated tool, and volume and shape for each structure were compared between groups.

Results. PDD and DLB patients showed global subcortical atrophy compared to PD patients. Greater hippocampal atrophy was the specific trait that distinguished PDD from PD, while greater atrophy of the pallidi discriminated DLB from PDD. Vertex analysis revealed specific shape differences in both structures.

Conclusions. Our results suggest that automated, time-sparing, subcortical volumetry may provide diagnostically useful information in α-synucleinopathies. Future studies on larger samples and with iron-sensitive MRI contrasts are needed.

INTRODUCTION

Abnormal accumulation of inclusions containing α-synuclein is the neuropathological hallmark of synucleinopathies, e.g. Parkinson disease (PD), Dementia with Lewy bodies (DLB) and Parkinson Disease Dementia (PDD), among others. The pathological hallmarks of these three conditions are the loss of dopaminergic neurons in the substantia nigra along with inclusions of Lewy bodies and Lewy neurites. Lewy bodies' deposition is thought to start in the medulla oblongata and progress to diencephalic, telencephalic and cortical structures in the final stages of PD [1].

Clinical findings reflect the ascending spreading of pathology: extrapyramidal features of PD are related to basal ganglia involvement in early disease stages, while cognitive complaints in PDD and DLB are thought to be a consequence of cortical Lewy body burden [2, 3].

When extrapyramidal and cognitive symptoms occur in close succession, classification between PDD and DLB becomes difficult. The most widely used diagnostic criteria in this context is the "one year role": a case is classified as DLB if dementia occurs within one year from motor symptom onset, whereas it is diagnosed as PDD if dementia is identified more than one year after motor symptom onset [4]. However, the existence of PDD and DLB as two distinct entities is still a matter of debate; it has been shown that the severity of Lewy body distribution in PDD and DLB is comparable, and cognitive assessment and clinical progression follow a similar trajectory in both diseases [5-8]. Conversely, whole-brain volumetric MRI studies have found differential patterns of cortical involvement between PDD and DLB [9, 10]. Measures of cortical atrophy in PD are inconclusive when compared to those in age-matched controls [10, 11]; only structural measurements of the basal ganglia have shown some promise [12-16]. Despite some already existing evidence of basal ganglia involvement in the transition from PD to PD-MCI [17-19], studies comparing subcortical atrophy patterns between PD and PDD are limited [20, 21].

In this study, we tested two hypotheses: (i) whether subcortical volumes might characterise PD-dementia (PDD) relative to PD, and (ii) whether PDD and DLB might be distinguished by their subcortical atrophy pattern. To this end, we studied both global (volumetric) and regional (shape based) measurements of atrophy in several subcortical structures using a validated, fully-automated segmentation method for structural MRI.

METHODS

Subjects. Patients were consecutively recruited at the Centre for Ageing Brain and Neurodegenerative Disorders and the Centre for Movement Disorders of the Neurology Unit, Department of Clinical and Experimental Sciences, University of Brescia, Italy and at S. Isidoro Hospital - FERB Onlus, Trescore Balneario, Bergamo, Italy.

A diagnosis of probable PD was made according to the Queen Square Brain Bank clinical criteria [22], defined by the presence of bradykinesia and at least one between muscular rigidity, rest tremor or postural instability. Diagnosis of PD was further accomplished by documented response to levodopa and absence of cognitive impairment on the basis of standardized neuropsychological assessment. Diagnosis of PDD was made in those patients fulfilling PD criteria, who developed multi-domain dementia more than one year after diagnosis of PD, according to the MDS criteria [23, 24]. DLB diagnosis was made in those patients who developed parkinsonism and cognitive decline at onset, fulfilling the DLB consortium clinical criteria for probable DLB [4].

In order to rule out a probable Alzheimer's Disease diagnosis, each DLB patient underwent DATSCAN SPECT imaging, which showed reduced bilateral striatal dopaminergic binding [4].

Each patient underwent general and neurological examination, neuropsychological assessment and brain structural MRI scanning. Patients were followed-up for at least one year to ensure a more consistent clinical diagnosis.

Stringent exclusion criteria were applied as follows: 1) cerebrovascular disorders, previous stroke, normal pressure hydrocephalus, and intra-cranial mass lesions documented by MRI; 2) diagnosis of other type of neurodegenerative disorders (i.e., Multiple System Atrophy, Corticobasal Syndrome, Progressive Supranuclear Palsy) according to current clinical criteria; 3) other neurological disorders or significant medical problems (i.e. hepatic or renal failure, chronic respiratory insufficiency) potentially responsible for encephalopathy; or 4) use of antipsychotic treatment or iatrogenic parkinsonism. The work conformed to the Helsinki Declaration and patients were enrolled according to the Local Ethics Committee criteria and with appropriate informed consent.

Clinical, behavioural and neuropsychological assessment. Staging of PD, PDD and DLB motor symptoms was assessed by the Unified Parkinson Disease Rating Scale, motor part (UPDRS-III). Behavioural disturbances were recorded according to the Neuropsychiatric Inventory [25]. A comprehensive neuropsychological and behavioural assessment, including Basic Activities of Daily Living (BADL) and Instrumental Activities of Daily Living (IADL), was carried out. Neuropsychological testing was performed by a standardized neuropsychological battery including Mini-Mental State Examination (MMSE), Rey Auditory Verbal Learning Test (RAVLT), Rey Complex Figure Copy and Recall, Stroop Color-Word Test, Phonological and Category Fluency, Visual Object and Space Perception Battery (VOSP) subtests (Number Location; Cube Analysis; Silhouette and Progressive Silhouettes), Trail Making Test A and B and Clock Drawing Test [26].

MRI data, acquisition and processing. All imaging was obtained using a 1.5 Tesla Siemens Avanto magnetic resonance scanner (Siemens, Erlangen, Germany), equipped with a circularly polarized single channel transmit-receive coil.

In a single session, the following scans were collected from each studied subject: (1) T2-weighted TSE scan (TR/TE=2500ms/50ms) to exclude the presence of macroscopic brain abnormalities, according to exclusion criteria; 2) 3D magnetization-prepared rapid gradient echo (MPRAGE) T1-weighted scan (TR=2050 ms, TE=2.56 ms, inversion time=1100 ms, Matrix=1x1x1 mm^3, in-plane field of view FOV=256x256x256 mm^3, flip angle =15°).

Preprocessing steps included conversion of DICOM images to NIFTI format and reorientation to MNI 152 space.

Segmentation of grey matter (GM), white matter (WM) and cerebro-spinal fluid (CSF) was performed in the native space, to obtain the Total Intracranial Volume (defined as the sum of GM, WM and CSF) and the Total Brain Volume (defined as the sum of GM and WM) which were subsequently used to normalize subcortical volumes [27]. We used the Advanced Data Processing Assistant for Resting-State fMRI (DPARSFA) (http://rfmri.org/DPARSF) with the "Unified Segmentation" option, which relies on SPM8 scripts.

Segmentation of subcortical structures was performed with the fully-automated FMRIB's Integrated Registration and Segmentation Tool (FIRST), implemented in FSL 5.0 [28]. The following regions were segmented: caudate, putamen, pallidus, thalamus, amygdala, accumbens and hippocampus, bilaterally. FIRST registers a model composed of manually segmented volumes of 336 subjects (healthy and pathological subjects ranging from 4 to 87 years of age, provided by the Center for Morphometric Analysis, MGH, Boston) to each subject's T1 image.

It uses a two-stage affine process to register each brain image onto an MNI 152 template. The first stage of this registration is performed on the whole brain. In the second stage, this intermediate brain image is weighted by a subcortical mask and affine registration is applied one more time in order to achieve optimal registration of the subcortical structures. Once the registration is estimated, inverse transformation is calculated and applied to the MNI 152 template to bring it to the native space so that the original image voxels do not have to be interpolated. After a general registration is achieved, Bayesian Active Appearance Model (AAM) is used to register and segment each subcortical structure precisely. AAM is an extension of Active Shape Model (ASM) [29] and it incorporates intensity information in addition to the geometrical shape model [30].

FIRST creates a surface mesh for each subcortical structure using a deformable mesh model. Each mesh is made up of triangles and the apex of connecting triangles represents a vertex [15, 28]. In this way, FIRST allows for both an estimation of volume and shape of each structure.

Comparing FIRST segmentation to manual segmentation (considered as the gold standard) with a leave-one-out (LOO) cross-validation method, Patenaude et al. found a good concordance among the two methods, ranging from 0.7 and 0.9. Best concordance was found for thalamus and putamen, while smaller structures such as accumbens and amygdala showed a lower median Dice overlap [28].

Each subject's segmentation output was visually inspected using the "first_slice_dir" script, but no gross inaccuracies were identified.

Statistical analysis

Differences in clinical and demographic data among groups were assessed using one-way ANOVA or chi-square test, as appropriate. For continuous variables, Bonferroni post-hoc test was performed to assess differences among paired groups. Values of p<0.05 were considered significant.

For imaging analysis, the volume of each structure was extracted. TIV and TBV were calculated in order to normalize each subcortical volume to head size. Normalized subcortical volumes (reported in mm^3) were calculated with the following formula: (average TIV of the total population * (total brain or subcortical volume of the participant/TIV of the participant)) [27].

Then, the mean between the left and right volume of each structure was considered, and differences for each structure were probed with a multivariate analysis of equal mean where age, gender and disease duration were nuisance factors.

Values of p<0.05, Fisher's least significant difference (LSD) post-hoc corrected, were considered significant.

For shape analysis, we adopted the *ReconNative+RigidAlign* option, which reconstructs the meshes in the native space of the images. It removes the pose with a 6 degree-of-freedom (DOF) registration, retaining both volume and shape. Statistical analysis was performed using two-sample t-tests (PD vs PDD and PDD vs DLB), with age, gender and disease duration as nuisance variables. P-values <0.05 corrected for the false discovery rate were considered significant [31].

RESULTS

As reported in **Table 1**, our cohort of patients consisted of 16 PD, 11 PDD and 16 DLB patients.

PD patients were cognitively unimpaired as compared to both PDD and DLB.

PDD patients were younger at disease onset and had a longer disease course as compared to DLB patients.

Results from volumetric analysis are summarised in **Table 2.** PDD and DLB patients returned significantly smaller volumes in the whole brain, caudati, pallidi, accumbens nuclei, thalami and hippocampi compared to the PD group.

When we considered the differences between PD and PDD, the regions found to be the most affected were caudati, accumbens nuclei, thalami and hippocampi. The logistic regression analysis revealed that hippocampus was the only significant predictor differentiating PD and PDD ($p < 0.001$, $\beta = 0.688$), thus being the best predictor of PD-related dementia (see **Figure 1**, panel A)

When comparing PDD and DLB, the only significant difference was found in the pallidi; these being more impaired in DLB (**Figure 1**, panel B).

We then performed shape analysis in the most predictive regions, namely the hippocampus (PD vs PDD) and globus pallidus (PDD vs DLB) (see **Figure 2**, panel A and B).

Both left and right hippocampi showed supra-threshold differences in the PDD < PD contrast, with left hippocampus being extensively affected by regional atrophy in its dorsolateral and ventrolateral surfaces. No significant shape alterations were found for the opposite contrast (PDD greater than PD).

DLB patients showed deformation of both dorsal and ventral pallidal surface when compared to PDD. No significant deformations in the PDD < DLB contrast were found.

DISCUSSION

In this work, our aim was to study subcortical differences in the three most common alpha-synucleinopathies. PD, PDD and DLB are characterised by the same neuropathological substrate, and overlapping clinical symptoms [32]. Dementia occurs in about 85% of PD patients over disease course [23], and PDD and DLB may be distinguished only by the controversial "one year rule" criterion [4]. To unravel differences between these disorders, we focused on the basal ganglia.

Different neuropathological studies in the PD spectrum have demonstrated that the striatum is commonly affected by α-synuclein pathology, with higher burden and co-occurrence of Aβ and Tau deposition in the striatum of PDD and DLB patients [5, 33, 34]. Among these two groups, DLB patients seem to be more severely and frequently affected [34].

We used FIRST, an algorithm implemented in FSL, which enables fast automated segmentation of several subcortical structures with good accuracy and reliability [28]. As compared to manual segmentation, actually considered the gold standard, software like FIRST and FreeSurfer have shown to provide good estimates of subcortical volumes, particularly with higher intraclass correlation coefficient (ICC) for larger structures [35, 36]. With regard to FIRST, high inter- and intra-scanner reliability has been demonstrated, proposing it as a robust and computationally rapid alternative to FreeSurfer segmentation [37].

Two main results were obtained by the present study. First, we observed the selective involvement of hippocampus in the transition from PD to PD-dementia. Preferential involvement of this region can be justified both by neuritic dystrophy in limbic structures and by the possible co-occurrence of Alzheimer's disease pathology and cholinergic dysfunction [38].

The second finding was the evidence of PDD and DLB differences at subcortical level. Indeed, in PDD patients, despite extensive cortical and subcortical atrophy, the only preserved structure was the pallidus, whose volume was comparable to that of PD patients. Globus pallidus is known to be the major output of the basal ganglia circuitry: it receives both dopaminergic (from substantia nigra and ventral tegmental area), and cholinergic inputs, and projects to thalamic nuclei and back to the cortex [39, 40]. At our knowledge, only one previous neuropathological work explored globus pallidus in DLB

and PDD in a series of 34 patients. The authors showed only one isolated DLB case with Aß plaques in the pallidus, and none of the PDD patients [34].

PDD and DLB are the focus of the on-going debate whether they are in essence the same disorder or they represent truly distinct phenotypes. The present results, along with previous structural and functional MRI works exploring cortical structures [9, 10], might be supportive of the latter hypothesis.

In conclusion, the results of this pilot study, if confirmed, argued that probing subcortical structures with structural MRI might be useful to define PD patients at-risk for dementia and to discriminate between PDD and DLB condition in uncertain cases.

However, some limitations should be acknowledged. First of all, the small sample of subjects and the necessity to covariate for parameters known to influence brain volumes (i.e. age, gender, disease duration) greatly limits the statistical power. In order to confirm these results, larger samples are required.

Furthermore, despite the careful patients' selection and acquisition of DATSCAN imaging to define DLB pathology, this study lacks of neuropathological confirmation.

Finally, it is worth discussing a technical point: the caveat that the pallidum—together with the amygdala and nucleus accumbens—are the least reliable structures for automated segmentation [28]. The issue of segmenting the pallidum with a T1-weighted contrast is that it is one of the most iron-rich grey matter structures in the adult brain [41], thereby its grey/white matter contrast is poorer compared with e.g. the cortex. In fact, there is evidence suggesting that iron accumulation might drive mis-segmentation of basal ganglia structures from structural scans due to T1-shortening [42]; thus, it is at least conceivable the present results might also reflect increased metal accumulation in DLB's pallidum. Future research, utilising more specific iron-sensitive MRI contrasts such as quantitative susceptibility mapping (QSM) and/or R2* mapping, might shed some light on this observation.

Disclosure of conflict of interest

On behalf of all authors, the corresponding author states that there is no conflict of interest.

Table 1. Clinical, demographic and neuropsychological characteristics of the cohort

	PD (16)	PDD (11)	DLB (16)	p	p^	p*	p†
Gender, F%	18.8 (3)	18.2 (2)	43.8 (7)	0.204[a]			
Age	69.4±4.7	71.6±5.6	74.4±5.9	0.042	-	0.037	-
Age of onset	62.3±6.1	62.1±8.9	70.3±6.5	0.003	-	0.007	0.014
Years of disease	7.2±3.0	9.5±6.1	4.1±3.0	0.005	-	-	0.004
UPDRS-III	12.7±6.8	28±10.6	20.1±8.5	<0.001	<0.001	-	-
Cognition assessment							
MMSE	28.1±1.8	18.4±3.5	20.9±5.6	<0.001	<0.001	<0.001	-
RAVLT, immediate	45.4±7.1	25.0±5.7	29.3±8.9	<0.001	<0.001	<0.001	-
RAVLT, recall	9.8±2.4	3.5±2.5	4.2±3.0	<0.001	<0.001	<0.001	-
CRF, copy	30.5±3.5	9.6±7.6	13.1±10.6	<0.001	<0.001	<0.001	-
CRF, recall	16.9±5.4	6.0±4.1	6.2±6.2	<0.001	0.002	<0.001	-
Clock's drawing	8.1±2.1	3.4±2.1	4.1±2.1	<0.001	<0.001	<0.001	-
Fluency, semantic	43.6±8.3	24.3±3.7	26.3±7.2	<0.001	<0.001	<0.001	-
Fluency, phonological	34.8±9.1	19.0±9.8	24.7±9.2	<0.001	<0.001	0.014	-
TMT, part A	37.6±23.3	327.3±143.0	296.7±194.7	<0.001	<0.001	<0.001	-
TMT, part B	169.3±175.6	389.4±61.2	388.8±125.7	<0.001	0.002	0.001	-
Stroop test, time	15.4±10.2	48.6±38.2	40.0±29.2	0.009	0.015	0.05	-
Stroop test, error	0.1±0.3	9.6±6.5	11.4±8.9	<0.001	0.003	<0.001	-
VOSP, numer location	7.9±2.5	5.0±3.2	3.7±2.6	<0.001	0.03	<0.001	-
VOSP, cube analysis	8.6±2.1	3.6±2.0	3.1±2.2	<0.001	<0.001	<0.001	-
VOSP, silhouettes	18.9±4.3	11.6±4.1	10.7±3.0	<0.001	<0.001	<0.001	-
VOSP, progressive silhouettes	10.6±2.9	6.7±3.8	8.5±3.9	0.031	0.029	-	-

One-way ANOVA, otherwise specified: [a]chi-square test. Results are expressed as mean ± standard deviation. Gender is expressed as percentage, number of subjects between brackets.

p^, p* and p† refer to post-hoc comparison (Bonferroni). p^ = PD vs PDD; p* = PD vs DLB; p† = PDD vs DLB.

UPDRS-III: Unified Parkinson's Disease Rating Scale, part III. MMSE: Mini-Mental State Examination.

RAVLT: Rey Auditory Verbal Learning Test. VOSP: Visual Object and Space Perception Battery. CRF: Complex Rey Figure. TMT: Trail Making Test.

Table 2. Cortical and subcortical volumes of the cohort

	PD	PDD	DLB	p	p^	p†
TBV	$1094 \times 10^3 \pm 53 \times 10^3$	$1006 \times 10^3 \pm 61 \times 10^3$	$976 \times 10^3 \pm 69 \times 10^3$	<0.001	0.001	-
Caudate, L	3153±264	2781±278	2904±380	0.008	0.002	-
Caudate, R	3198±278	3015±331	2876±332	-	-	-
Caudate, mean	3176±260	2899±215	2891±330	0.031	0.013	-
Putamen, L	4349±502	4049±366	4058±412	-	-	-
Putamen, R	4264±498	4105±413	4003±416	-	-	-
Putamen, mean	4307±477	4078±341	4031±366	-	-	-
Pallidus, L	1647±178	1709±294	1519±153	-	-	-
Pallidus, R	1665±145	1631±203	1444±211	0.014	-	0.014
Pallidus, mean	1657±145	1670±235	1482±173	0.049	-	0.02
Accumbens, L	427±135	327±88	304±130	-	0.036	-
Accumbens, R	351±112	238±91	201±107	0.001	0.02	-
Accumbens, mean	389±107	283±67	253±109	0.005	0.011	-
Thalamus, L	7203±511	6688±578	6717±474	0.04	0.017	-
Thalamus, R	7052±445	6599±481	6514±428	0.019	0.018	-
Thalamus, mean	7128±460	6644±517	6615±407	0.02	0.012	-
Hippocampus, L	3759±602	2825±520	3193±371	<0.001	<0.001	0.03
Hippocampus, R	3855±632	3281±460	3213±471	0.028	0.02	-
Hippocampus, mean	3808±505	3053±452	3204±351	<0.001	<0.001	-
Amygdala, L	1438±228	1334±217	1364±147	-	-	-
Amygdala, R	1486±200	1454±256	1274±262	-	-	-
Amygdala, mean	1462±192	1395±209	1319±190	-	-	-

Multivariate analysis, considering age, gender and disease duration as nuisance variables. Volumes are expressed as mean ± standard deviation (mm^3).

p^ and p† refer to post-hoc comparison (LSD). p^ = PD vs PDD; p† = PDD vs DLB.

L: left. R: right. TBV: total brain volume.

Figure 1. Box plots of hippocampal and pallidal volumes in α-synucleinopathies.

Panel A: comparison between hippocampal volumes of PD and PDD subjects

Panel B: comparison between pallidal volumes of PDD and DLB subjects

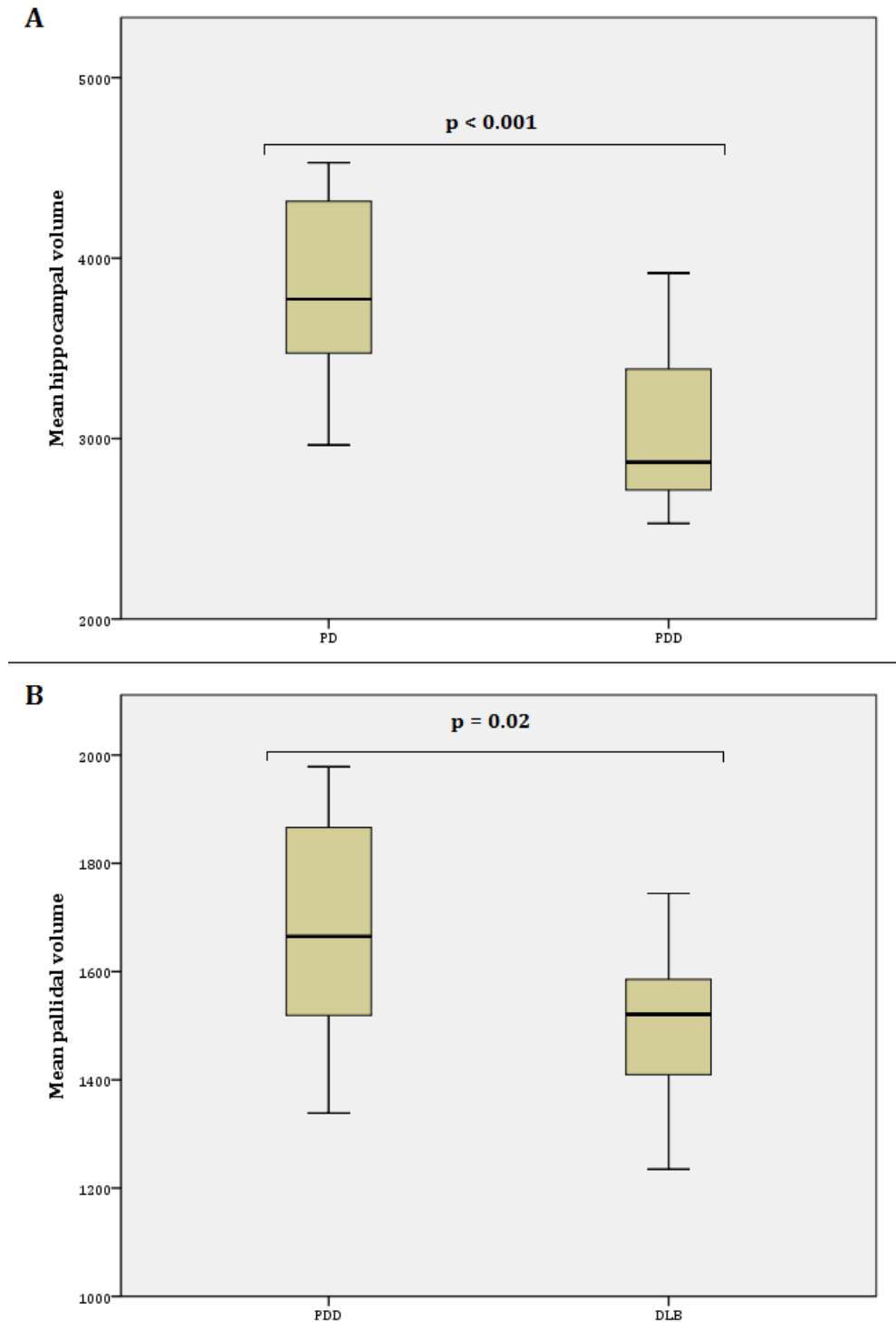Box: mean volume of the structure in mm³. Plot: standard deviation in mm³

Figure 2. Shape analysis of hippocampi and pallidi in α-synucleinopathies.

Panel A: dorsal and ventral view of left and right hippocampus in the PDD < PD contrast.

Panel B: dorsal and ventral view of left and right globus pallidus in the DLB < PDD contrast.

Light blue: structure shape; orange: shape difference. P < 0.05 FDR corrected.

A: anterior. P: posterior. L: left. R: right.
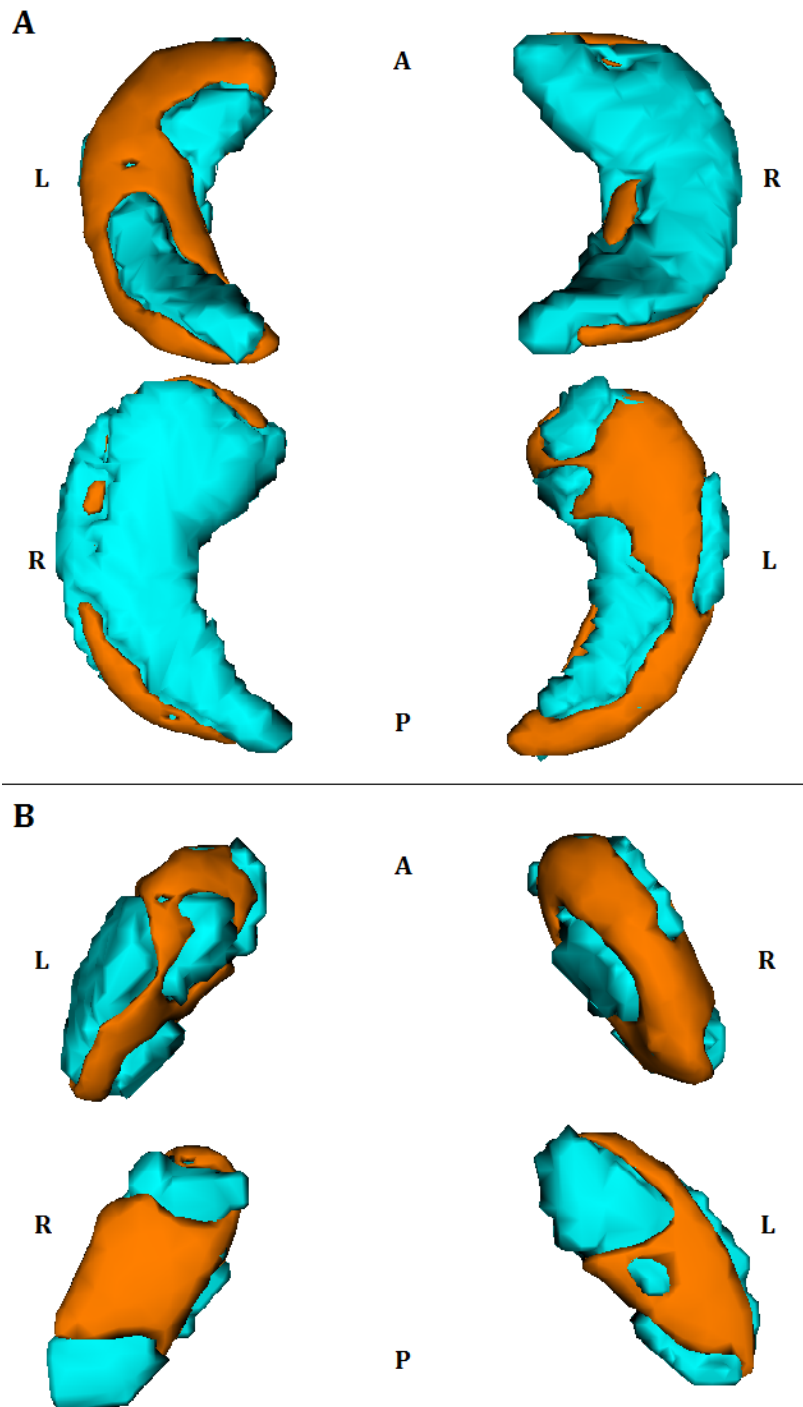
[1].   Braak H, Del Tredici K, Rub U, de Vos RA, Jansen Steur EN, Braak E. Staging of brain pathology related to sporadic Parkinson's disease. *Neurobiol Aging*. 2003 **24:** 197-211.

[2].   Emre M. Dementia associated with Parkinson's disease. *Lancet Neurol*. 2003 **2:** 229-237.

[3].   Hurtig HI, Trojanowski JQ, Galvin J*, et al.* Alpha-synuclein cortical Lewy bodies correlate with dementia in Parkinson's disease. *Neurology*. 2000 **54:** 1916-1921.

[4].   McKeith IG, Dickson DW, Lowe J*, et al.* Diagnosis and management of dementia with Lewy bodies: third report of the DLB Consortium. *Neurology*. 2005 **65:** 1863-1872.

[5].   Tsuboi Y, Dickson DW. Dementia with Lewy bodies and Parkinson's disease with dementia: are they different? *Parkinsonism Relat Disord*. 2005 **11 Suppl 1:** S47-51.

[6].   Guo L, Itaya M, Takanashi M, Mizuno Y, Mori H. Relationship between Parkinson disease with dementia and dementia with Lewy bodies. *Parkinsonism Relat Disord*. 2005 **11:** 305-309.

[7].   Goldman JG, Williams-Gray C, Barker RA, Duda JE, Galvin JE. The spectrum of cognitive impairment in Lewy body diseases. *Mov Disord*. 2014 **29:** 608-621.

[8].   Aarsland D, Ballard CG, Halliday G. Are Parkinson's disease with dementia and dementia with Lewy bodies the same entity? *J Geriatr Psychiatry Neurol*. 2004 **17:** 137-145.

[9].   Beyer MK, Larsen JP, Aarsland D. Gray matter atrophy in Parkinson disease with dementia and dementia with Lewy bodies. *Neurology*. 2007 **69:** 747-754.

[10].   Borroni B, Premi E, Formenti A*, et al.* Structural and functional imaging study in dementia with Lewy bodies and Parkinson's disease dementia. *Parkinsonism Relat Disord*. 2015 **21:** 1049-1055.

[11].   Planetta PJ, Kurani AS, Shukla P*, et al.* Distinct functional and macrostructural brain changes in Parkinson's disease and multiple system atrophy. *Hum Brain Mapp*. 2015 **36:** 1165-1179.

[12].   Menke RA, Szewczyk-Krolikowski K, Jbabdi S*, et al.* Comprehensive morphometry of subcortical grey matter structures in early-stage Parkinson's disease. *Hum Brain Mapp*. 2014 **35:** 1681-1690.

[13].   Garg A, Appel-Cresswell S, Popuri K, McKeown MJ, Beg MF. Morphological alterations in the caudate, putamen, pallidum, and thalamus in Parkinson's disease. *Front Neurosci*. 2015 **9:** 101.

[14].   Sterling NW, Du G, Lewis MM*, et al.* Striatal shape in Parkinson's disease. *Neurobiol Aging*. 2013 **34:** 2510-2516.

[15].   Nemmi F, Sabatini U, Rascol O, Peran P. Parkinson's disease and local atrophy in subcortical nuclei: insight from shape analysis. *Neurobiol Aging*. 2015 **36:** 424-433.

[16].   Lee HM, Kwon KY, Kim MJ*, et al.* Subcortical grey matter changes in untreated, early stage Parkinson's disease without dementia. *Parkinsonism Relat Disord*. 2014 **20:** 622-626.

[17].   Melzer TR, Watts R, MacAskill MR*, et al.* Grey matter atrophy in cognitively impaired Parkinson's disease. *J Neurol Neurosurg Psychiatry*. 2012 **83:** 188-194.

[18].   Mak E, Bergsland N, Dwyer MG, Zivadinov R, Kandiah N. Subcortical atrophy is associated with cognitive impairment in mild Parkinson disease: a combined investigation of volumetric changes, cortical thickness, and vertex-based shape analysis. *AJNR Am J Neuroradiol*. 2014 **35:** 2257-2264.

[19].   Pereira JB, Junque C, Bartres-Faz D, Ramirez-Ruiz B, Marti MJ, Tolosa E. Regional vulnerability of hippocampal subfields and memory deficits in Parkinson's disease. *Hippocampus*. 2013 **23:** 720-728.

[20].   Apostolova LG, Beyer M, Green AE*, et al.* Hippocampal, caudate, and ventricular changes in Parkinson's disease with and without dementia. *Mov Disord*. 2010 **25:** 687-695.

[21].   Mak E, Su L, Williams GB, O'Brien JT. Neuroimaging correlates of cognitive impairment and dementia in Parkinson's disease. *Parkinsonism Relat Disord*. 2015 **21:** 862-870.

[22].   Hughes AJ, Daniel SE, Kilford L, Lees AJ. Accuracy of clinical diagnosis of idiopathic Parkinson's disease: a clinico-pathological study of 100 cases. *J Neurol Neurosurg Psychiatry*. 1992 **55:** 181-184.

[23].   Emre M, Aarsland D, Brown R*, et al.* Clinical diagnostic criteria for dementia associated with Parkinson's disease. *Mov Disord*. 2007 **22:** 1689-1707; quiz 1837.

[24].   Goetz CG, Emre M, Dubois B. Parkinson's disease dementia: definitions, guidelines, and research perspectives in diagnosis. *Ann Neurol*. 2008 **64 Suppl 2:** S81-92.

[25].   Cummings JL, Mega M, Gray K, Rosenberg-Thompson S, Carusi DA, Gornbein J. The Neuropsychiatric Inventory: comprehensive assessment of psychopathology in dementia. *Neurology*. 1994 **44:** 2308-2314.

[26].   Lezak MD. *Neuropsychological assessment*. 3rd edn. New York: Oxford University Press, 1995.

[27].   van Norden AG, Fick WF, de Laat KF*, et al.* Subjective cognitive failures and hippocampal volume in elderly with white matter lesions. *Neurology*. 2008 **71:** 1152-1159.

[28].   Patenaude B, Smith SM, Kennedy DN, Jenkinson M. A Bayesian model of shape and appearance for subcortical brain segmentation. *Neuroimage*. 2011 **56:** 907-922.

[29].   Taylor CJ, Cootes TF, Lanitis A, Edwards G, Smyth P, Kotcheff AC. Model-based interpretation of complex and variable images. *Philos Trans R Soc Lond B Biol Sci*. 1997 **352:** 1267-1274.

[30].   Sandman CA, Head K, Muftuler LT, Su L, Buss C, Davis EP. Shape of the basal ganglia in preadolescent children is associated with cognitive performance. *Neuroimage*. 2014 **99:** 93-102.

[31].   Genovese CR, Lazar NA, Nichols T. Thresholding of statistical maps in functional neuroimaging using the false discovery rate. *Neuroimage*. 2002 **15:** 870-878.

[32].   Berg D, Postuma RB, Bloem B*, et al.* Time to redefine PD? Introductory statement of the MDS Task Force on the definition of Parkinson's disease. *Mov Disord*. 2014 **29:** 454-462.

[33].   Tsuboi Y, Uchikado H, Dickson DW. Neuropathology of Parkinson's disease dementia and dementia with Lewy bodies with reference to striatal pathology. *Parkinsonism Relat Disord*. 2007 **13 Suppl 3:** S221-224.

[34].   Jellinger KA, Attems J. Does striatal pathology distinguish Parkinson disease with dementia and dementia with Lewy bodies? *Acta Neuropathol*. 2006 **112:** 253-260.

[35].   Morey RA, Petty CM, Xu Y*, et al.* A comparison of automated segmentation and manual tracing for quantifying hippocampal and amygdala volumes. *Neuroimage*. 2009 **45:** 855-866.

[36].   Morey RA, Selgrade ES, Wagner HR, 2nd, Huettel SA, Wang L, McCarthy G. Scan-rescan reliability of subcortical brain volumes derived from automated segmentation. *Hum Brain Mapp*. 2010 **31:** 1751-1762.

[37].   Nugent AC, Luckenbaugh DA, Wood SE, Bogers W, Zarate CA, Jr., Drevets WC. Automated subcortical segmentation using FIRST: test-retest reliability, interscanner reliability, and comparison to manual segmentation. *Hum Brain Mapp*. 2013 **34:** 2313-2329.

[38].   Ruffmann C, Calboli FC, Bravi I*, et al.* Cortical Lewy bodies and Abeta burden are associated with prevalence and timing of dementia in Lewy body diseases. *Neuropathol Appl Neurobiol*. 2015.

[39].   Hegeman DJ, Hong ES, Hernandez VM, Chan SC. The External Globus Pallidus: Progress and Perspectives. *Eur J Neurosci*. 2016.

[40].   Gittis AH, Berke JD, Bevan MD*, et al.* New roles for the external globus pallidus in basal ganglia circuits and behavior. *J Neurosci*. 2014 **34:** 15178-15183.

[41].   Acosta-Cabronero J, Betts MJ, Cardenas-Blanco A, Yang S, Nestor PJ. In Vivo MRI Mapping of Brain Iron Deposition across the Adult Lifespan. *J Neurosci*. 2016 **36:** 364-374.

[42].   Goto M, Abe O, Miyati T*, et al.* Association between iron content and gray matter missegmentation with voxel-based morphometry in basal ganglia. *J Magn Reson Imaging*. 2013 **38:** 958-962.